



CHORUS

This is the accepted manuscript made available via CHORUS. The article has been published as:

## Structural and vibrational properties of methane up to 71 GPa

Maxim Bykov, Elena Bykova, Chris J. Pickard, Miguel Martinez-Canales, Konstantin Glazyrin, Jesse S. Smith, and Alexander F. Goncharov

Phys. Rev. B **104**, 184105 — Published 8 November 2021

DOI: [10.1103/PhysRevB.104.184105](https://doi.org/10.1103/PhysRevB.104.184105)

# Structure and vibrational properties of methane up to 71 GPa

Maxim Bykov<sup>1,2</sup>, Elena Bykova<sup>1</sup>, Chris J. Pickard<sup>3,4</sup>, Miguel Martinez-Canales<sup>5</sup>,  
Konstantin Glazyrin<sup>6</sup>, Jesse S. Smith<sup>7</sup>, Alexander F. Goncharov<sup>1</sup>

<sup>1</sup>Earth and Planets Laboratory, Carnegie Institution of Washington, 5251 Broad Branch Road  
Washington D.C., USA

<sup>2</sup>Howard University, 2400 6<sup>th</sup> St NW, Washington DC 20059, USA

<sup>3</sup>Department of Materials Sciences & Metallurgy, University of Cambridge, Cambridge, UK

<sup>4</sup>Advanced Institute for Materials Research, Tohoku University, Aoba, Sendai, 980-8577, Japan

<sup>5</sup>School of Physics & Astronomy, The University of Edinburgh, Edinburgh, UK

<sup>6</sup>Photon Sciences, Deutsches Electronen Synchrotron (DESY), D-22607 Hamburg, Germany

<sup>7</sup>HPCAT, X-ray Science Division, Argonne National Laboratory, Argonne, IL 60439, USA

**Single-crystal synchrotron X-ray diffraction, Raman spectroscopy, and first principles calculations have been used to identify the structure of the high-pressure (HP) phase of molecular methane above 20 GPa up to 71 GPa at room temperature. The structure of HP phase is trigonal  $R\bar{3}$ , which can be represented as a distortion of the cubic phase B, previously documented at 7-15 GPa and confirmed here. The positions of hydrogen atoms in HP phase have been obtained from first principles calculations, which also demonstrated the stability of this structure above 260 K at 25 GPa. The molecules occupy four different crystallographic sites in phases B and eleven sites in the HP phase, which result in splitting of molecular stretching modes detected in Raman spectroscopy and assigned here based on a good agreement with the Raman spectra calculated from the first principles. Our study points out to a single HP phase unlike up to three HP phases proposed previously based on the Raman spectroscopy results only.**

## Introduction

Methane represents a rare and fundamental example of hydrogen-bearing molecular compound with no hydrogen bonds unlike other simple molecules HF, H<sub>2</sub>O, H<sub>2</sub>S, and NH<sub>3</sub>. Thus, the crystal structure formation in methane solids is expected to be mainly determined by the steric effects and

33 van der Waals bonds, suggesting that its behavior at high pressure may be similar to the rare gas  
34 solids, for example Ar <sup>1</sup>, which persists in a face-centered cubic (*fcc*) structure to very high  
35 pressures. Furthermore, the high-pressure behavior of methane is of interest to explore possible  
36 deviations from simple closed packed structures and related to this molecular orientational  
37 ordering, where the hydrogen atoms find the most energetically favorable stable positions. The  
38 fate of methane at even higher compression states in the regime of molecular proximity (i.e.  
39 shortened intermolecular H-H distances) is of great interest as it can be considered as a hydrogen  
40 dominant alloy <sup>2</sup> with the relevance to high-temperature superconductivity <sup>3</sup>. In addition, the  
41 behavior of methane at high pressures and temperatures may be of interest because it is believed  
42 to be a valued component of the deep planetary interiors of “icy” giant planets such as Uranus and  
43 Neptune <sup>4</sup>. Such hot molecular ices of water and ammonia form superionic crystals with diffusive  
44 protons at extreme pressure-temperature (P-T) conditions of relevance for these planets <sup>5-7</sup>, while  
45 methane tends to chemically react yielding oligomeric hydrocarbon compounds <sup>8</sup> and dissociate at  
46 higher P-T conditions yielding diamond and hydrogen <sup>9-11</sup>.

47         Similar to Ar, methane crystallizes in phase I at about 1.5 GPa upon compression at room  
48 temperate forming a face-centered cubic (*fcc*) closed packed structure of the molecular centers at  
49 the carbon atoms <sup>12</sup>, and this crystal is plastic - molecules are freely rotating. However, unlike in  
50 noble gases, this structure transforms at 5.4 GPa to a complex rhombohedral structure A with 21  
51 molecules in the unit cell solved by a combination of single crystal neutron and X-ray diffraction  
52 (XRD) techniques <sup>13</sup>. The structure is rhombohedrally distorted from the *fcc* methane I, with the  
53 carbon atoms occupying nine different crystallographic positions, and some of them may be  
54 associated with orientationally ordered molecules. However, the Raman and IR spectra do not  
55 show the obvious splitting of the major  $\nu_1$  and  $\nu_3$  C-H stretching modes <sup>14</sup>.

56         Further compression leads to a transition to phase B with a very large unit cell containing  
57 58 molecules, which has been found cubic as solved recently by Maynard-Casely *et al.* <sup>15</sup> for the  
58 carbon subsystem by combining powder and single-crystal XRD. The phase B shows a splitting  
59 of  $\nu_1$  and  $\nu_3$  stretching C-H modes in IR and Raman spectra <sup>1, 14, 16, 17</sup>, suggesting that it possesses  
60 some elements of orientational order (*e.g.* Refs. <sup>14, 16</sup>). The transition from phase A to phase B at  
61 about 8 GPa is very sluggish and phase B can be missed if fast compressed yielding a simple cubic  
62 phase pre-B <sup>16</sup>, where the Raman active  $\nu_1$  and  $\nu_3$  C-H stretching modes are not split suggesting  
63 that methane molecules are orientationally disordered. Phase B is reported to transform to a high

64 pressure phase 1 (HP1) at about 25 GPa manifested by anomalies in IR spectra, vibrational  
65 frequencies<sup>18</sup>, and specific volume<sup>19</sup>, while no drastic structural changes were detected in the  
66 powder diffraction patterns. At higher pressures, Raman spectroscopy observations suggest further  
67 structural modifications to HP2 and HP3 phases reported up to 62 GPa<sup>16</sup>; however, the transition  
68 pressures to the subsequent high-pressure phases are contradictory<sup>16, 17</sup>. The structure of the HP  
69 phase(s) has not been solved; it has been postulated to be cubic (*e.g.* Ref. <sup>20</sup>), but no detailed  
70 structural information is available. The XRD experiments have been extended to 202 GPa and the  
71 volume has been determined based on a cubic symmetry, even though a major transformation has  
72 been detected and a volume discontinuity was found at 94 GPa<sup>20</sup>. Methane was reported to persist  
73 in a molecular crystal structure beyond 200 GPa<sup>20, 21</sup>.

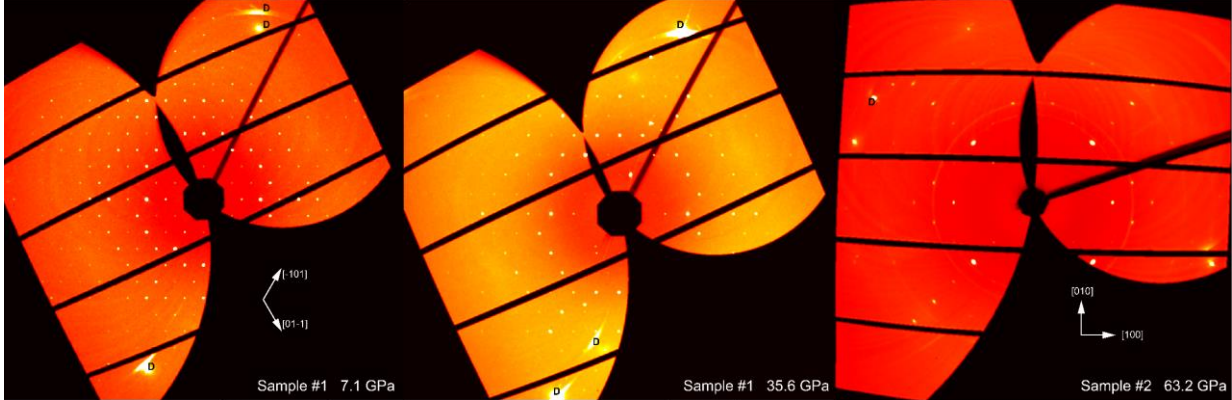
74 In this paper, we examine the structure of methane in the pressure range between 7 and 71  
75 GPa using single-crystal XRD, Raman spectroscopy, and first-principles theoretical calculations.  
76 Our single-crystal XRD data directly determine the structure of the carbon subsystem in agreement  
77 with the previous report in phase B<sup>15</sup>, while we find that HP phase can be viewed as  
78 rhombohedrally distorted phase B (space group *R3*) with 87 molecules in the unit cell (29 in the  
79 primitive unit cell); this structure remains unchanged between 20 and 73 GPa. We applied *ab initio*  
80 random structure search<sup>22</sup> of the most stable structures with and without any restriction of the  
81 symmetry. The results yield the structure of HP phase in agreement with XRD data, and determine  
82 the hydrogen positions in HP phase. The Raman spectrum of this phase calculated from the first  
83 principles is in a qualitative agreement with the experiment demonstrating that the C-H stretching  
84 mode splitting is due to a variation in the crystal field at different crystallographic sites.

85

## 86 **Experimental and theoretical procedures**

87 Methane gas was loaded in a mixture with He gas at approximately 1:1 mole ratio compressed to  
88 0.15 GPa at room temperature in a BX90 diamond anvil cell<sup>23</sup> (Fig. S1 of the Supplemental  
89 Material<sup>24</sup>). In order to obtain good-quality single crystals of phase B of methane, the gas mixture  
90 was slowly compressed at 297 K through the methane solidification point at 1.5 GPa and then to  
91 8 GPa. At this pressure, excellent single crystals of phase B were grown overnight judging on  
92 Raman observations of a splitting of the  $\nu_1$  C-H stretch mode (Fig. S2 of the Supplemental Material  
93 <sup>24</sup>). These crystals yield very sharp Bragg reflections with typical rocking-curve width of 0.64° at  
94 7.1 GPa (Fig. 1). Two samples (#1 and #2) were compressed up to 39 GPa and 71 GPa respectively

95 and concomitant XRD and Raman spectroscopy measurements (Figs. 1, 2 and Fig. S2 of the  
96 Supplemental Material <sup>24</sup>) were taken at selected pressure points. All the experiments were  
97 performed at room temperature (295(2) K).



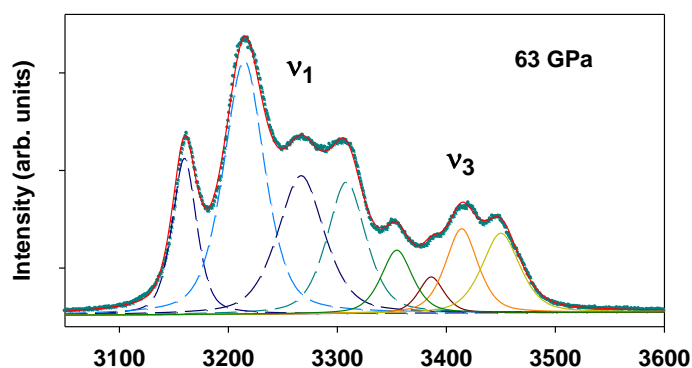
108 **Figure 1.** Reconstructed reciprocal lattice plane of methane visualized by CrysAlisPro software  
109 package<sup>25</sup> at 7.07 GPa (left), 35.6 GPa (middle) and 63.2 GPa (right). **D** stands for diamond  
110 reflections. The observed diffraction spots from the sample have been indexed and used to  
111 determine the structure of phases B (left panel) and high-pressure (HP) phase (middle and right  
112 panel) (Table S1 and Tables 1, 2, respectively).

113 X-ray diffraction was performed at the beamlines 16-ID-B (APS, Argonne, USA) and  
114 P02.2 (Petra III, DESY, Hamburg, Germany). The following beamline setups were used. P02.2:  $\lambda$   
115 = 0.289 Å, beam size  $\sim 2 \times 2 \mu\text{m}^2$ , Perkin Elmer XRD 1621 detector; 16-ID-B:  $\lambda$  = 0.344 Å, beam  
116 size  $\sim 3 \times 3 \mu\text{m}^2$ , Pilatus 1M detector. For the single-crystal XRD measurements samples were  
117 rotated around a vertical  $\omega$ -axis in a range  $\pm 22^\circ$ . The diffraction images were collected with an  
118 angular step  $\Delta\omega = 0.5^\circ$  and an exposure time of 2-10 s/frame. For analysis of the single-crystal  
119 diffraction data (indexing, data integration, frame scaling and absorption correction) we used the  
120 *CrysAlis<sup>Pro</sup>* software package<sup>25</sup>. To calibrate an instrumental model in the *CrysAlis<sup>Pro</sup>* software,  
121 *i.e.*, the sample-to-detector distance, detector's origin, offsets of goniometer angles, and rotation  
122 of both X-ray beam and the detector around the instrument axis, we used a single crystal of  
123 orthoenstatite ((Mg<sub>1.93</sub>Fe<sub>0.06</sub>)(Si<sub>1.93</sub>, Al<sub>0.06</sub>)O<sub>6</sub>, *Pbca* space group,  $a = 8.8117(2)$ ,  $b = 5.18320(10)$ ,  
124 and  $c = 18.2391(3)$  Å). The same calibration crystal was used at both beamlines. The structure was  
125 solved with the ShelXT structure solution program<sup>26</sup> using intrinsic phasing and refined with the

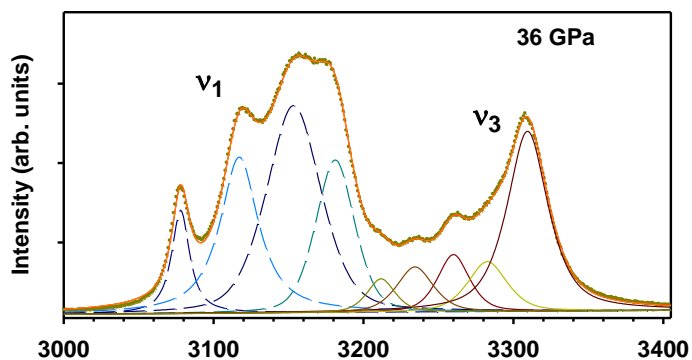
126 Jana 2006 program <sup>27</sup>. Raman spectra were collected using the GSECARS Raman System<sup>28</sup> with  
127 the excitation wavelength of 532 nm and at the Earth and Planets Laboratory of Carnegie (EPL)  
128 using a 488 nm excitation line (e.g. Ref. <sup>29</sup>). Pressure was determined based on the shift of the R1  
129 ruby fluorescence line <sup>30</sup>.

130

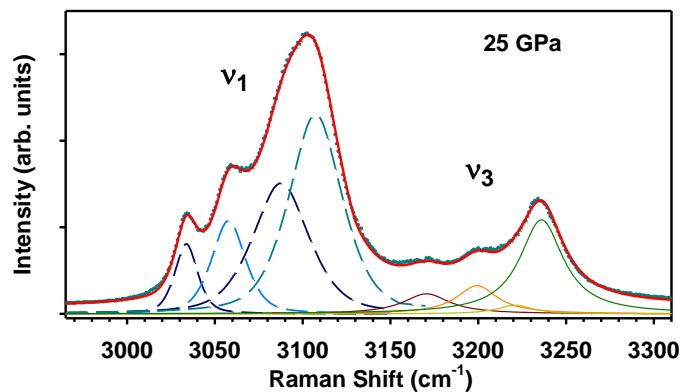
131



137



143



149

150 **Figure 2. Raman spectra of the C-H stretching modes of methane in HP phase at various**  
151 **pressures.** The dots are the data and the lines are the fits to the Voigt oscillator model with eight  
152 (nine for the 36 GPa spectrum) peaks; variable color lines show the individual  $\nu_1$  (dashed) and  $\nu_3$   
153 (solid) components. Note a change in the frequency scale in different panels due to a pressure shift.

154 Ab Initio Random Structures Searches (AIRSS)<sup>31</sup> were performed using the CASTEP code  
 155 <sup>22</sup> to explore the structures of the HP methane with the rhombohedral symmetry (the unit cells with  
 156 up to 87 atoms were explored), with a subsequent relaxation using density functional theory (DFT)  
 157 calculations within the CASTEP code <sup>22</sup>. Raman spectra were computed using density functional  
 158 perturbation theory (DFPT) + Finite differences method, using the default CASTEP 18 NC  
 159 pseudopotentials with a 1250 eV energy cutoff, and a similarly dense k-point grid.

160

## 161 **Results and discussion**

162 At pressures below ~16 GPa, the diffraction pattern of CH<sub>4</sub> (Fig. 1) can be indexed with a body-  
 163 centered cubic unit cell of phase B (Table S1 and Fig. S3 <sup>24</sup>). Structure solution and refinement is  
 164 in agreement with the model reported by Maynard-Casely *et al.* <sup>15</sup>. Due to weak scattering of  
 165 hydrogen atoms, we were able to refine the positions of carbon atoms only. The unit cell contains  
 166 four independent atomic sites: C1, C2, C3, and C4 occupying the positions *2a*, *24g*, *8c* and *24g*,  
 167 respectively. Therefore, there are 58 CH<sub>4</sub> molecules in the unit cell.

168 Further compression leads to a noticeable lattice distortion at above 18 GPa and the unit  
 169 cell can no longer be considered cubic. This distortion is accompanied by the appearance of new  
 170 modes in the Raman spectrum (Figs. 2 and Fig. S2 of the Supplemental Material <sup>24</sup>) in agreement  
 171 with the previous observations <sup>16,17</sup> at similar pressure conditions. The most plausible indexing of  
 172 the diffraction patterns of a methane high-pressure phase (HP) above 18 GPa can be performed  
 173 using a rhombohedral unit cell (Tables 1, 2). Symmetry-lowering transitions from cubic *I*-43*m* to  
 174 rhombohedral symmetry may follow  $\Gamma_4$  or  $\Gamma_5$  irreducible representations with the following  
 175 transformation of the lattice parameters:

$$176 \begin{pmatrix} \mathbf{a}_R \\ \mathbf{b}_R \\ \mathbf{c}_R \end{pmatrix} = \begin{pmatrix} -1 & 1 & 0 \\ 0 & -1 & 1 \\ 1/2 & 1/2 & 1/2 \end{pmatrix} \begin{pmatrix} \mathbf{a}_c \\ \mathbf{b}_c \\ \mathbf{c}_c \end{pmatrix},$$

177 where  $\mathbf{a}_R$ ,  $\mathbf{b}_R$ ,  $\mathbf{c}_R$  are lattice vectors of the rhombohedral unit cell (hexagonal setting), while  $\mathbf{a}_c$ ,  $\mathbf{b}_c$ ,  
 178  $\mathbf{c}_c$ - lattice vectors of the cubic unit cell. The  $\Gamma_4$  distortion leads to the space group symmetry *R3m*  
 179 (#160), while  $\Gamma_5$  - to *R3* (#146). We should note that at pressures above 30 GPa we see a slight  
 180 departure of the lattice parameters from *R*-centered hexagonal lattice ( $a = b$ ,  $\alpha = \beta = 90^\circ$ ,  $\gamma = 120^\circ$ )  
 181 suggesting a further monoclinic distortion. However, the degree of this distortion is not  
 182 reproducible between two experiments (Fig. S4). Therefore, we conclude that this effect is related

183 to the development of non-hydrostatic stresses in the sample, which is unavoidable at very high  
184 pressures and especially for very soft crystals like methane. We therefore treat the high-pressure  
185 phase of methane as a single *R3* phase.

186 We have tested both *R3* and *R3m* models (Table 1). Although the *R3* model has smaller  
187 agreement factors, they are not significantly different from those of the *R3m* model. We have  
188 performed a Hamilton significance test in order to check if the improvement of the agreement  
189 factors for the *R3* model may be considered significant<sup>32</sup>. For this test, both models were refined  
190 using the same set of reflections averaged based on the *R3* symmetry. Based on the Hamilton test,  
191 the *R3* model is preferable with the 75-90 % confidence level depending on the pressure point.  
192 We, therefore, cannot completely reject the *R3m* model based on the XRD data, but can conclude  
193 that the *R3* model is more likely (Table 1).

194 In order to complete the structure solution and determine the positions of hydrogen atoms,  
195 theoretical structure optimizations have been performed at various pressures (Fig. 3). First, we  
196 performed ab initio Random Structure Search (AIRSS) using the CASTEP code<sup>22</sup>. All calculations  
197 used the PBE functional together with the DFT-D dispersion correction scheme of Tkatchenko and  
198 Scheffler<sup>33</sup>. Among a plethora of phases marginally different in enthalpies, two structures emerged  
199 having *R3* symmetries and 29 molecules in the primitive unit cell (*R3*-I and *R3*-II on the Fig. 2(a))  
200 in agreement with the experimental HP phase (Fig. 4). Both calculated *R3* structures have  
201 equivalent carbon substructures and slightly different orientations of CH<sub>4</sub> molecules centered at  
202 the C4 atoms. According to the theoretical calculations both *R3* structures are not the most  
203 energetically favorable at 0 K. However, if temperature effects are taken into account, the  
204 calculated Gibbs free energies show that the *R3*-II phase becomes the most favorable above 260  
205 K at 25 GPa, which perfectly agrees with the experiment (Figure 3(b)). A monoclinic distortion  
206 noticed experimentally is found to be energetically unfavorable. Below we will mainly discuss  
207 the most energetically favorable *R3* phase (*R3*-II, Table 3).

208

209

210

211

212

213

214

215

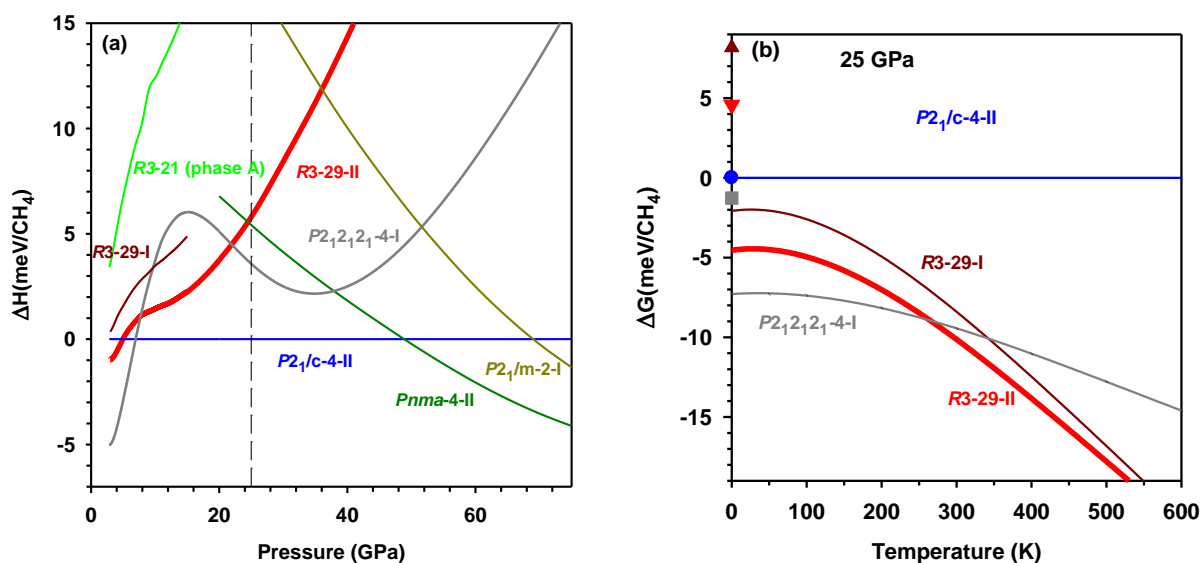
216

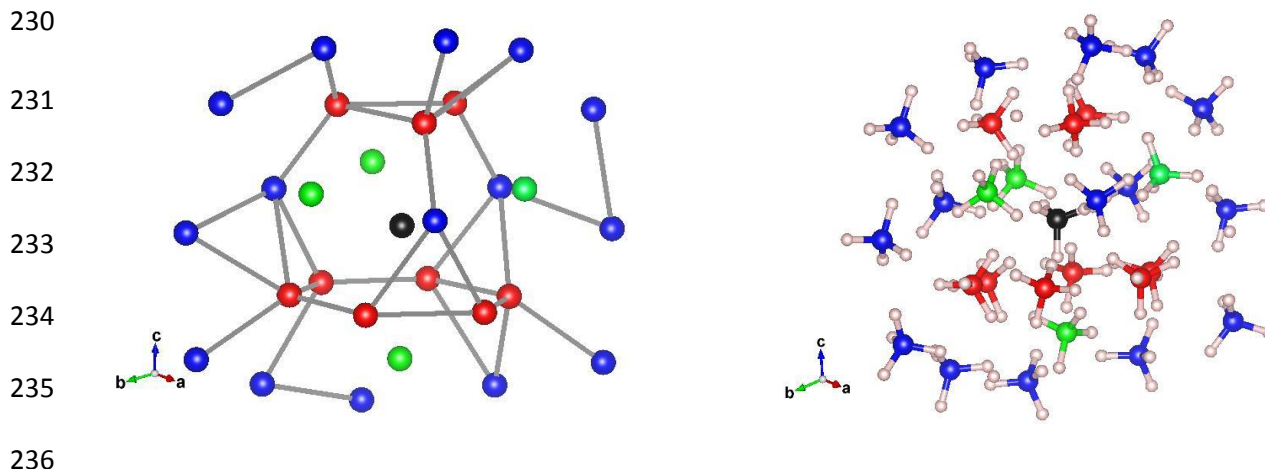
217 **Figure 3.** (a) Theoretically calculated relative enthalpy of the most stable methane phases. The  
218 results for HP phase (*R3-II*) are shown by a thick red line. Other orientationally ordered phases are  
219 shown by thin lines of various colors. The vertical dashed line correspond to the pressure at which  
220 the temperature effects were taken into account (b) Relative Gibbs free energies of the most stable  
221 methane phases as a function of temperature at 25 GPa. The symbols at  $T=0$  K represent relative  
222 classical enthalpies as computed with norm-conserving pseudo potentials.

223

224 The unit cell of HP-CH<sub>4</sub> (Fig. 4 and Fig. S5 of the Supplemental Material<sup>24</sup>) contains 11 symmetry  
225 independent carbon atoms with atoms C1\_1 and C3\_1 occupying positions  $3a$ , while the rest  
226 occupying positions  $9b$ . Here, the C atoms are named following the numbering for phase B<sup>15</sup> to  
227 show the relation between B and HP phases, *i.e.* the atom C3\_1 is generated from the atom C3 of  
228 the B-phase.

229





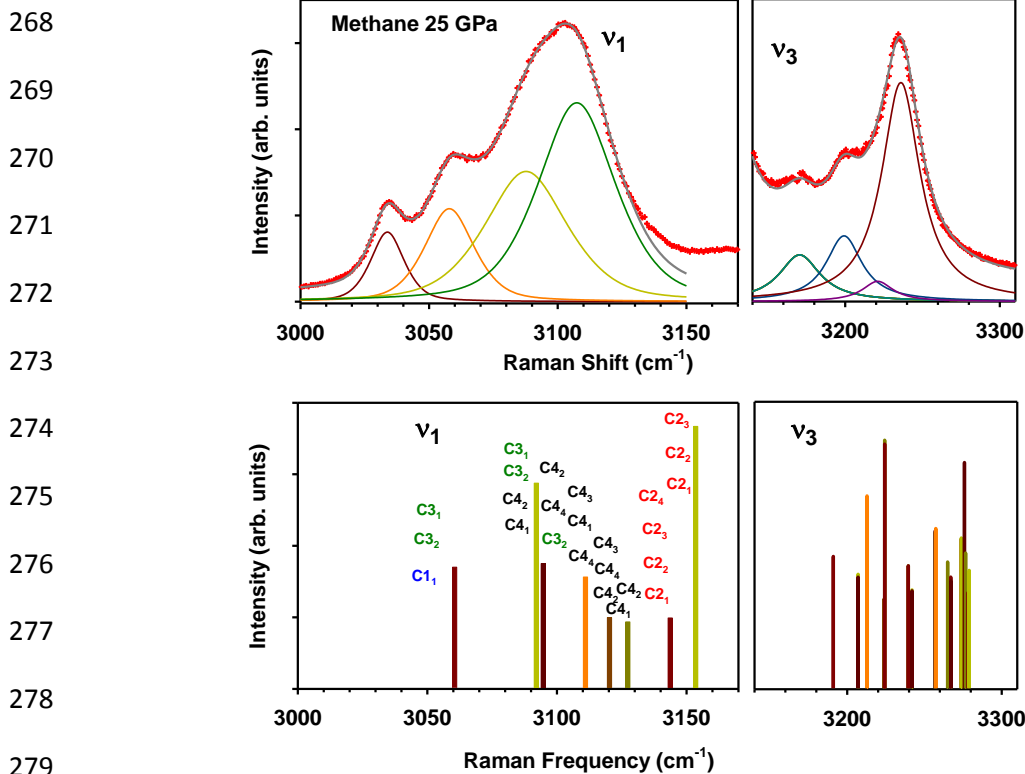
237 **Figure 4.** Crystal structure of HP-CH<sub>4</sub> at 35 GPa. Black, red, green and blue balls represent the  
238 positions of C1, C2, C3, and C4 carbon atoms, respectively; small pinkish circles are hydrogen  
239 atoms. Left panel shows C atoms only; gray lines connect the nearest C atoms with a cutoff of 3.08  
240 Å.

241 Figure 4 shows the main motif of the most energetically favorable *R3* structure. The C1\_1  
242 and C3\_1 atoms that lie on the three-fold axis possess a distorted tetrahedral icosi-octahedral  
243 environment. This polyhedron can be understood in the following way (see bottom of the Fig. S5  
244 <sup>24</sup>): the atom C3\_1 is coordinated by two six-membered rings, one of which is planar and capped,  
245 while the other is in a chair arrangement capped by a triangle. The packing of HP-CH<sub>4</sub> is primarily  
246 defined by intermolecular H-H interactions. The histogram of H-H distances has two distinct peaks  
247 (Fig. S6 <sup>24</sup>). The sharp peak at ~1.75 Å corresponds to intramolecular H-H distances and almost  
248 does not shift with pressure as the molecules remain almost rigid under compression. The broad  
249 maxima at ~2.05 and ~1.95 Å at 20 and 30 GPa, respectively, correspond to closest intermolecular  
250 H...H contacts. These distances are in a good agreement with shortest intramolecular H...H  
251 contacts in compressed hydrogen <sup>34</sup>.

252 The  $\nu_1$  and  $\nu_3$  C-H stretching Raman modes become composite (see also Refs. <sup>16, 17</sup>) in  
253 phases B and HP suggesting either site symmetry or vibrational splitting. The Raman spectra  
254 collected at 25 GPa in HP phase show that each of the  $\nu_1$  and  $\nu_3$  multifold can be well represented  
255 by 4 peaks (Figs. 2, 5) except at 36 GPa, where an additional weak fifth peak tentatively assigned  
256 to the  $\nu_3$  fundamental is seen. On the other hand, theoretical calculations of the Raman activity of  
257 HP phase performed in this work show a larger number of components, which correspond to

258 various molecular sites as the analysis for the  $\nu_1$  modes shows (Fig. 5). However, the splitting  
 259 pattern and value are qualitatively similar to the experimental; moreover, some theoretically  
 260 calculated peaks are very close to each other making them difficult to resolve in the experiment;  
 261 this likely results in broadened peaks, which consist of many components. A prominent feature of  
 262 the  $\nu_1$  Raman spectra is a well split off low frequency peak, that theory predicts is due internal  
 263 vibrations of molecules involving C1 and C3 carbon in  $3a$  sites, which are characterized by  
 264 relatively more uniform in length and overall longer intermolecular distances (Fig. S7<sup>24</sup>). This  
 265 distinction results in a well-separated low-frequency  $\nu_1$  component, which can be also seen in  
 266 phase B with similar carbon site geometry save the lattice distortion.

267



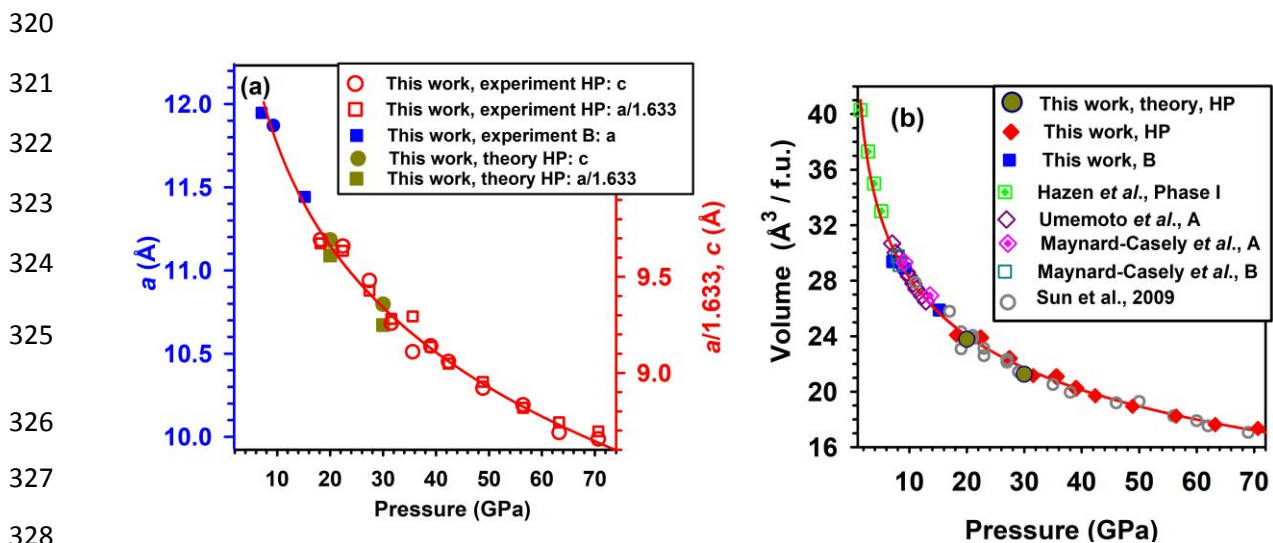
280 **Figure 5.** Raman spectra of  $\nu_1$  (left panels) and  $\nu_3$  (right panels) stretching modes. The top panels  
 281 is the spectrum measured at 25 GPa (488 nm excitation). Crosses are the data and gray line is the  
 282 best fit to the Voigt oscillator model; variable color lines show the individual  $\nu_1$  and  $\nu_3$  components.  
 283 The bottom panel shows the theoretically computed spectra at the same pressure. The labels  
 284 (carbon atom sites) show the assignment of the peaks to the molecules of different kind. The

285 experimental and theoretical peaks in the top and the bottom panels only slightly mismatch  
286 demonstrating a good correspondence of experiment and theory.

287

288 The unit-cell parameters and symmetry of phases B and HP obtained here experimentally and  
289 theoretically provide reliable information on the P-V equation of state of methane (Fig. 6). Our  
290 results agree well with the previous determinations based on single-crystal<sup>13, 15</sup> and powder<sup>19, 20,</sup>  
291<sup>35</sup> XRD. The cubic unit cell of phase B shows a distortion in the HP phase, which first appears  
292 small but then increases with pressure (Fig. S4<sup>24</sup>). Please note that pre-B phase, which appears on  
293 fast compression of phase A, was indexed as a simple cubic lattice<sup>19, 20</sup>; this phase is not examined  
294 with XRD here (but was detected by Raman spectroscopy to coexist with HP phase in the  
295 experiment #2 up to the highest pressure investigated) but it is clearly different from HP phase of  
296 this study. HP and pre-B methane phases have very close volumes per the formula unit (Fig. 6) if  
297 one assumes that pre-B has 21 molecules in the unit cell as in phase A. Unlike previously reported  
298 modifications of HP phase based on changes in a number of  $\nu_1$  and  $\nu_3$  Raman components<sup>16, 17</sup>,  
299 our direct structural data (Fig. 1, Tables 1-2) and analysis indicate that there exists only a single  
300 HP phase up to 71 GPa (cf. Refs.<sup>16, 17</sup>), where the rhombohedral distortion gradually increases  
301 with pressure (Fig. S4<sup>24</sup>). Consistently, we also find (by fitting the spectra using an oscillator  
302 models, Figs. 2, 5) that the number of C-H Raman components remains essentially the same (cf.  
303 Refs.<sup>16, 17</sup>) and their frequencies (Fig. 7) agree well with the results of previous Raman  
304 investigations<sup>16, 17</sup>. The pressure dependencies of all the Raman frequencies can be approximated  
305 by sublinear curves (Fig. 7). Previous Raman investigations<sup>16, 17</sup> reported minor changes in the  
306 spectra (peak splitting and changes in peak intensities) and in the P dependence of the C-H stretch  
307 frequencies. However, these changes do not signify the phase transitions, and, moreover, the  
308 inferred phase boundaries were inconsistent between these two investigations. The Raman peaks  
309 may split because they consist of a number of components, which have different pressure slopes  
310 so they become separated with pressure, while their relative intensity may change due to a number  
311 of reasons including the mode coupling and modification in the orientational order.

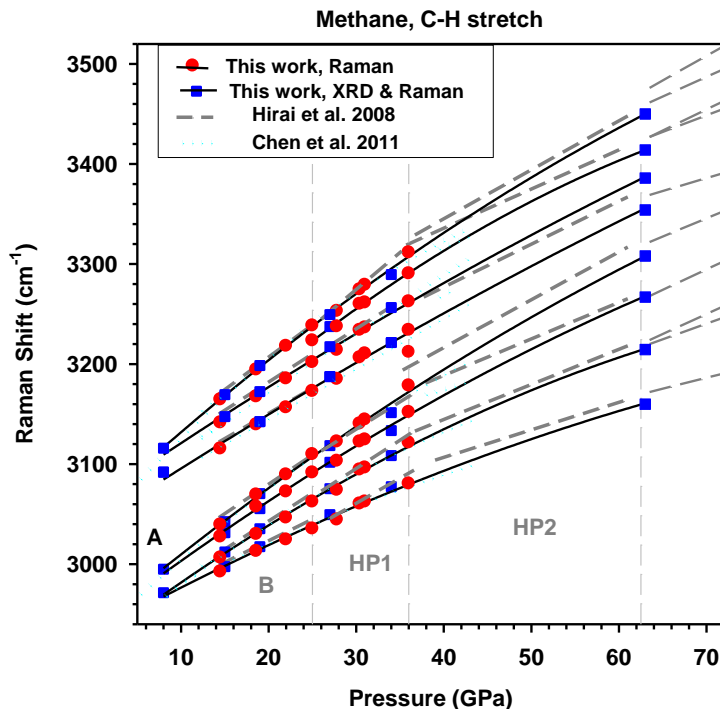
312 The unit cell volume changes smoothly through the B-HP transition suggesting a very small or no  
 313 discontinuity. The theoretically computed lattice parameters and volumes are smaller than those  
 314 determined theoretically, but the discrepancy is within 3%, which commonly is considered  
 315 acceptable. However, this small difference may indicate that HP methane may still be partially  
 316 disordered, which also corroborate with smaller (by some 20%) observed values of  $v_1$  and  $v_3$   
 317 multifolds splitting compared to the computed ones (Fig. 5). It is also worth noting that the  
 318 measured and calculated Raman frequencies agree quite well, within 1.5%, demonstrating the  
 319 validity of approximations made for computing the Raman spectra.



329 **Figure 6.** Lattice parameters (a) and volumes per formula unit (b) of methane as a function of  
 330 pressure. Note two vertical scales in the panel (a) for phases B (blue) and HP (red) which are scaled  
 331 by a factor of  $\sqrt{3}/2$  reflecting the difference in the unit cell dimensions. Also, the parameter  $a$  of  
 332 the HP phase is divided by a factor of 1.633. Our experimental and theoretical volumes (b) are  
 333 compared to previous experiments in phases I, A, B, and HP<sup>12, 13, 15, 19, 20</sup>. The unit cell volume of  
 334 Ref.<sup>20</sup> was assumed to contain 21 formula units. The lines are guides to the eye.

335  
 336  
 337  
 338

339  
340  
341  
342  
343  
344  
345  
346  
347  
348



349 **Figure 7. Raman frequencies of the C-H stretching modes of methane as a function of**  
350 **pressure.** Vertical dashed lines mark the phase transitions following Ref. <sup>16</sup>. The symbols are the  
351 results of two experiments of this work (solid line is the guide to the eye), while dashed and dotted  
352 lines represent the results of previously published works <sup>16, 17</sup>. The data between 36 and 63 GPa  
353 could not be taken because the experiment to 63 GPa was performed at the X-ray synchrotron  
354 beamline, so the Raman spectra could be only measured at the last pressure point.

355

## 356 Conclusions

357 Our concerted experimental and theoretical investigation determined the structure of the high-  
358 pressure HP phase of methane including the positions of hydrogen atoms. The structure is  
359 rhombohedral (space group  $R3$ ) with 87 molecules in the unit cell. This extraordinary complex  
360 structure of approximately spherical molecules is in a drastic contrast with simple  $fcc$  ( $hcp$ )  
361 structures of noble gas solids. Moreover, the theoretically predicted orientationally ordered  
362 structures with smaller unit cell and with well elaborated intermolecular coupling schemes also do  
363 not capture the real structure. This indicates that the observed structure represents a balance  
364 between enthalpy and entropy terms thus suggesting that some molecular sites remain

365 orientationally disordered; this makes this structure analogous to clathrates, where host and guest  
366 molecules are the same.

367 Our direct single-crystal XRD results suggest that there is only one high-pressure phase (HP) of  
368 methane between 20 and 71 GPa in contrast to previous works, which suggested up to three HP  
369 phase based on the results of Raman spectroscopy. HP phase investigated here can coexist with a  
370 cubic pre-B phase investigated previously, the detailed structure of which still remains unknown.

371

### 372 **Acknowledgements:**

373 Parts of this research were carried out at the Extreme Conditions Beamline (P02.2) at DESY, a  
374 member of Helmholtz Association (HGF). Portions of this work were performed at HPCAT (sector  
375 16) of the Advanced Photon Source (APS), Argonne National Laboratory. HPCAT operations are  
376 supported by DOE-NNSA's Office of Experimental Sciences. Concomitant Raman spectroscopy  
377 experiments were performed at GeoSoilEnviroCARS (The University of Chicago, Sector 13),  
378 Advanced Photon Source (APS), Argonne National Laboratory. GeoSoilEnviroCARS is supported  
379 by the National Science Foundation - Earth Sciences (EAR - 1634415) and Department of Energy  
380 GeoSciences (DE-FG02-94ER14466). The Advanced Photon Source is U.S. Department of  
381 Energy (DOE) Office of Science User Facility operated for the DOE Office of Science by Argonne  
382 National Laboratory under Contract No. DE-AC02-06CH11357. CJP acknowledges financial  
383 support from the Engineering and Physical Sciences Research Council [Grant EP/P022596/1]. MB  
384 research was sponsored by the Army Research Office and was accomplished under the  
385 Cooperative Agreement Number W911NF-19-2-0172.

386

387

388

389

390

391

392 **Table 1.** Comparison of agreement factors between *R3* and *R3m* models of the HP methane

| Pressure, GPa | # reflections | <i>R3</i> model |        | <i>R3m</i> model |        |
|---------------|---------------|-----------------|--------|------------------|--------|
|               |               | # parameters    | $R_1$  | # parameters     | $R_1$  |
| 22.4          | 381           | 41              | 0.127  | 28               | 0.1303 |
| 27.4          | 474           | 41              | 0.138  | 28               | 0.1422 |
| 35.6          | 280           | 41              | 0.1020 | 28               | 0.1033 |
| 39.0          | 198           | 41              | 0.1415 | 28               | 0.1436 |

393

394 **Table 2.** Crystal data, refinement and crystal structure details of Methane HP phase

| Pressure (GPa)   | 22.4                         | 27.4                   | 35.6                    | 39.0                           |
|--|------------------------------|------------------------|-------------------------|--------------------------------|
| <b>Crystal data</b>  |                              |                        |                         |                                |
| Crystal system, space group  | trigonal, <i>R3</i>          |                        |                         |                                |
| <i>Z</i>   | 87                           |                        |                         |                                |
| <i>a</i> , <i>c</i> (Å)  | 15.735(3),<br>9.660(2)       | 15.396(3),<br>9.481(2) | 15.176 (8),<br>9.11 (7) | 14.918(8),<br>9.14(7)          |
| <i>V</i> (Å <sup>3</sup> )   | 2071.3(7)                    | 1946.1(7)              | 1818(13)                | 1762(14)                       |
| Radiation type   | X-ray, $\lambda = 0.34453$ Å |                        |                         | X-ray,<br>$\lambda = 0.2891$ Å |
| $\mu$ (mm <sup>-1</sup> )  | 0.02                         | 0.02                   | 0.02                    | 0.02                           |
| <b>Data collection</b>   |                              |                        |                         |                                |
| Diffractometer   | GP @ ID16-B                  | GP @ ID16-B            | GP @ ID16-B             | GP @ P02.2                     |
| Absorption correction  | Multi-scan                   |                        |                         |                                |
| No. of measured, independent and observed [ $I > 3\sigma(I)$ ] reflections | 676, 663, 381                | 640, 627, 474          | 475, 365, 280           | 792, 587, 198                  |
| $R_{int}$  | 0.111                        | 0.026                  | 0.039                   | 0.059                          |
| $(\sin \theta/\lambda)_{max}$ (Å <sup>-1</sup> )                           | 0.752                        | 0.768                  | 0.586                   | 0.664                          |
| <b>Refinement</b>  |                              |                        |                         |                                |
| $R[F^2 > 2\sigma(F^2)]$ ,  | 0.127, 0.136,                | 0.138, 0.150,          | 0.102, 0.117,           | 0.141, 0.149,                  |

|   |            |             |             |             |
|---|------------|-------------|-------------|-------------|
| $wR(F^2), S$  | 3.14       | 5.70        | 3.61        | 1.60        |
| No. of reflections  | 663        | 627         | 365         | 587         |
| $\Delta\rho_{\max}, \Delta\rho_{\min}$ (e Å <sup>-3</sup> ) | 0.32/-0.28 | 0.36, -0.37 | 0.25, -0.19 | 0.23, -0.20 |
| <b>Crystal structure</b>                                    |            |             |             |             |
| <b>C1_1</b>   |            |             |             |             |
| x   | 0          | 0           | 0           | 0           |
| y   | 0          | 0           | 0           | 0           |
| z   | 0.02(12)   | 0.02(8)     | 0.000(17)   | 0.013(9)    |
| U <sub>iso</sub>  | 0.09(11)   | 0.090(12)   | 0.049(8)    | 0.033(4)    |
| <b>C2_1</b>   |            |             |             |             |
| x   | 0.0618(8)  | 0.0644(9)   | 0.0623(8)   | 0.0635(9)   |
| y   | 0.1264(8)  | 0.1264(9)   | 0.1234(9)   | 0.1251(8)   |
| z   | 0.33(12)   | 0.33(8)     | 0.340(16)   | 0.340(8)    |
| U <sub>iso</sub>  | 0.045(3)   | 0.035(3)    | 0.037(4)    | 0.050(3)    |
| <b>C2_2</b>   |            |             |             |             |
| x   | 0.4816(9)  | 0.4801(9)   | 0.4844(8)   | 0.4863(8)   |
| y   | 0.1468(9)  | 0.1451(9)   | 0.1485(8)   | 0.1476(7)   |
| z   | 0.17(12)   | 0.17(8)     | 0.165(15)   | 0.174(8)    |
| U <sub>iso</sub>  | 0.041(3)   | 0.028(3)    | 0.028(3)    | 0.046(3)    |
| <b>C2_3</b>   |            |             |             |             |
| x   | 0.6663(9)  | 0.6653(9)   | 0.6632(7)   | 0.6622(7)   |
| y   | 0.1458(9)  | 0.1477(9)   | 0.1483(7)   | 0.1495(7)   |
| z   | 0.17(12)   | 0.17(8)     | 0.162(16)   | 0.166(8)    |
| U <sub>iso</sub>  | 0.039(3)   | 0.028(3)    | 0.029(3)    | 0.041(3)    |
| <b>C2_4</b>   |            |             |             |             |
| x   | 0.1216(7)  | 0.1230(8)   | 0.1256(7)   | 0.1245(7)   |
| y   | 0.2456(7)  | 0.2449(8)   | 0.2489(6)   | 0.2506(7)   |
| z   | 0.09(12)   | 0.09(8)     | 0.101(16)   | 0.093(9)    |
| U <sub>iso</sub>  | 0.041(3)   | 0.035(3)    | 0.034(3)    | 0.046(3)    |
| <b>C3_1</b>   |            |             |             |             |
| x   | 0          | 0           | 0           | 0           |
| y   | 0          | 0           | 0           | 0           |
| z   | 0.67(12)   | 0.67(8)     | 0.666(16)   | 0.670(10)   |
| U <sub>iso</sub>  | 0.016(4)   | 0.014(4)    | 0.015(4)    | 0.049(6)    |
| <b>C3_2</b>   |            |             |             |             |
| x   | 0.2388(6)  | 0.2376(7)   | 0.2361(6)   | 0.2339(7)   |
| y   | 0.1208(6)  | 0.1174(7)   | 0.1178(6)   | 0.1175(7)   |
| z   | 0.14(12)   | 0.14(8)     | 0.152(15)   | 0.156(8)    |
| U <sub>iso</sub>  | 0.018(2)   | 0.014(2)    | 0.019(3)    | 0.039(3)    |
| <b>C4_1</b>   |            |             |             |             |
| x   | 0.4644(8)  | 0.4595(8)   | 0.4648(7)   | 0.4635(7)   |
| y   | -0.0756(7) | -0.0774(8)  | -0.0704(6)  | -0.0730(7)  |
| z   | 0.24(12)   | 0.24(8)     | 0.244(16)   | 0.239(8)    |
| U <sub>iso</sub>  | 0.047(3)   | 0.038(3)    | 0.036(3)    | 0.047(3)    |
| <b>C4_2</b>   |            |             |             |             |

|                  |            |            |           |           |
|------------------|------------|------------|-----------|-----------|
| x                | 0.0092(9)  | 0.0123(10) | 0.0065(9) | 0.0062(7) |
| y                | 0.3087(10) | 0.3130(11) | 0.3133(9) | 0.3104(7) |
| z                | 0.33(12)   | 0.33(8)    | 0.339(16) | 0.337(8)  |
| U <sub>iso</sub> | 0.050(4)   | 0.049(4)   | 0.036(3)  | 0.038(3)  |
| <b>C4_3</b>      |            |            |           |           |
| x                | 0.3005(8)  | 0.2991(10) | 0.3080(9) | 0.3070(7) |
| y                | 0.3121(9)  | 0.3081(11) | 0.3116(9) | 0.3122(7) |
| z                | 0.33(12)   | 0.33(8)    | 0.350(16) | 0.342(8)  |
| U <sub>iso</sub> | 0.047(4)   | 0.043(4)   | 0.037(3)  | 0.038(3)  |
| <b>C4_4</b>      |            |            |           |           |
| x                | 0.2294(8)  | 0.2239(10) | 0.2251(8) | 0.2230(8) |
| y                | 0.4529(8)  | 0.4531(10) | 0.4496(9) | 0.4481(8) |
| z                | 0.19(12)   | 0.18(8)    | 0.166(15) | 0.154(8)  |
| U <sub>iso</sub> | 0.038(3)   | 0.039(3)   | 0.030(3)  | 0.040(3)  |

395

396 **Table 3.** Crystal structure of HP-CH<sub>4</sub> at 25 GPa optimized by calculations (*R*3, *a* = 15.3315, *c* =  
397 9.5221 Å).

| Site   | <i>x</i>  | <i>y</i>  | <i>z</i>  |
|--------|-----------|-----------|-----------|
| C1_1   | 0         | 0         | -0.9996   |
| H1_1_1 | -0.365771 | -0.622456 | -0.628642 |
| H1_1_2 | 0         | 0         | -0.11349  |
| C2_1   | -0.131193 | -0.066507 | -0.68994  |
| H2_1_1 | -0.181504 | -0.146561 | -0.695142 |
| H2_1_2 | -0.083784 | -0.042373 | -0.781794 |
| H2_1_3 | -0.085473 | -0.048146 | -0.596947 |
| H2_1_4 | -0.174924 | -0.029387 | -0.685741 |
| C2_2   | 0.148245  | 0.474857  | -0.519002 |
| H2_2_1 | 0.079276  | 0.476659  | -0.509461 |
| H2_2_2 | 0.205456  | 0.534268  | -0.456087 |
| H2_2_3 | 0.136305  | 0.402921  | -0.484066 |
| H2_2_4 | -0.162001 | -0.181677 | -0.294102 |
| C2_3   | -0.183006 | 0.005534  | -0.191981 |
| H2_3_1 | -0.255161 | -0.062329 | -0.199231 |
| H2_3_2 | 0.144078  | -0.273369 | -0.461258 |
| H2_3_3 | -0.129179 | -0.010913 | -0.144596 |
| H2_3_4 | -0.157189 | 0.036738  | -0.29511  |
| C2_4   | -0.252732 | -0.13696  | -0.448695 |
| H2_4_1 | -0.285273 | -0.116555 | -0.534236 |
| H2_4_2 | -0.300828 | -0.15757  | -0.357472 |
| H2_4_3 | -0.243439 | -0.199203 | -0.480598 |
| H2_4_4 | -0.180176 | -0.073615 | -0.422955 |
| C3_1   | 0         | 0         | -0.346612 |
| H3_1_1 | 0.044147  | -0.032218 | -0.309195 |
| H3_1_2 | 0         | 0         | -0.460331 |

|        |           |           |           |
|--------|-----------|-----------|-----------|
| C3_2   | -0.096727 | -0.545671 | -0.549019 |
| H3_2_1 | 0.173063  | 0.094993  | -0.812157 |
| H3_2_2 | -0.079162 | -0.473773 | -0.593158 |
| H3_2_3 | -0.447561 | -0.266257 | -0.299235 |
| H3_2_4 | 0.299905  | 0.127484  | -0.823554 |
| C4_1   | -0.207481 | -0.422449 | -0.598684 |
| H4_1_1 | -0.274275 | -0.422628 | -0.563519 |
| H4_1_2 | -0.226509 | -0.496916 | -0.631667 |
| H4_1_3 | -0.173923 | -0.37107  | -0.685189 |
| H4_1_4 | -0.154241 | -0.399094 | -0.513821 |
| C4_2   | -0.322138 | -0.356324 | -0.361957 |
| H4_2_1 | -0.047361 | 0.238783  | -0.656792 |
| H4_2_2 | 0.083251  | 0.322741  | -0.659402 |
| H4_2_3 | -0.33452  | -0.297433 | -0.322463 |
| H4_2_4 | -0.323976 | -0.355022 | -0.47503  |
| C4_3   | -0.316752 | -0.01339  | -0.682065 |
| H4_3_1 | -0.308246 | 0.013518  | -0.575783 |
| H4_3_2 | 0.281839  | 0.313491  | -0.391824 |
| H4_3_3 | -0.252204 | 0.038722  | -0.743068 |
| H4_3_4 | 0.342394  | 0.246027  | -0.349393 |
| C4_4   | 0.214413  | 0.114945  | -0.509708 |
| H4_4_1 | 0.228418  | 0.190425  | -0.496222 |
| H4_4_2 | 0.141492  | 0.062025  | -0.467591 |
| H4_4_3 | 0.272312  | 0.106787  | -0.457289 |
| H4_4_4 | 0.214746  | 0.101117  | -0.620706 |

398

399

#### 400 References:

- 401 1. P. Hebert, A. Polian, P. Loubeyre and R. Le Toullec, *Physical Review B* **36** (17), 9196-  
402 9201 (1987).
- 403 2. N. W. Ashcroft, *Physical Review Letters* **92** (18), 187002 (2004).
- 404 3. E. Snider, N. Dasenbrock-Gammon, R. McBride, M. Debessai, H. Vindana, K.  
405 Vencatasamy, K. V. Lawler, A. Salamat and R. P. Dias, *Nature* **586** (7829), 373-377 (2020).
- 406 4. W. B. Hubbard, *Planetary interiors*. (Van Nostrand Reinhold, New York, N.Y., 1984).
- 407 5. C. Cavazzoni, G. L. Chiarotti, S. Scandolo, E. Tosatti, M. Bernasconi and M. Parrinello,  
408 *Science* **283** (5398), 44-46 (1999).
- 409 6. S. Ninet, F. Datchi and A. M. Saitta, *Physical Review Letters* **108** (16), 165702 (2012).
- 410 7. V. B. Prakapenka, N. Holtgrewe, S. S. Lobanov and A. Goncharov, arXiv:2007.07715v1  
411 [cond-mat.mtrl-sci] (2020).
- 412 8. S. S. Lobanov, P.-N. Chen, X.-J. Chen, C.-S. Zha, K. D. Litasov, H.-K. Mao and A. F.  
413 Goncharov, *Nature Communications* **4** (1), 2446 (2013).

- 414 9. F. Ancilotto, G. L. Chiarotti, S. Scandolo and E. Tosatti, *Science* **275** (5304), 1288-1290  
415 (1997).
- 416 10. D. Kraus, J. Vorberger, A. Pak, N. J. Hartley, L. B. Fletcher, S. Frydrych, E. Galtier, E. J.  
417 Gamboa, D. O. Gericke, S. H. Glenzer, E. Granados, M. J. MacDonald, A. J. MacKinnon, E. E.  
418 McBride, I. Nam, P. Neumayer, M. Roth, A. M. Saunders, A. K. Schuster, P. Sun, T. van Driel,  
419 T. Döppner and R. W. Falcone, *Nature Astronomy* **1** (9), 606-611 (2017).
- 420 11. G. Gao, A. R. Oganov, Y. Ma, H. Wang, P. Li, Y. Li, T. Iitaka and G. Zou, *The Journal*  
421 *of Chemical Physics* **133** (14), 144508 (2010).
- 422 12. R. M. Hazen, H. K. Mao, L. W. Finger and P. M. Bell, *Applied Physics Letters* **37** (3),  
423 288-289 (1980).
- 424 13. H. E. Maynard-Casely, C. L. Bull, M. Guthrie, I. Loa, M. I. McMahon, E. Gregoryanz, R.  
425 J. Nelmes and J. S. Loveday, *The Journal of Chemical Physics* **133** (6), 064504 (2010).
- 426 14. R. Bini, L. Ulivi, H. J. Jodl and P. R. Salvi, *The Journal of Chemical Physics* **103** (4),  
427 1353-1360 (1995).
- 428 15. H. E. Maynard-Casely, L. F. Lundegaard, I. Loa, M. I. McMahon, E. Gregoryanz, R. J.  
429 Nelmes and J. S. Loveday, *The Journal of Chemical Physics* **141** (23), 234313-234313 (2014).
- 430 16. H. Hirai, K. Konagai, T. Kawamura, Y. Yamamoto and T. Yagi, *Chemical Physics*  
431 *Letters* **454** (4-6), 212-217 (2008).
- 432 17. P.-N. Chen, C.-S. Zha, X.-J. Chen, J. Shu, R. J. Hemley and H.-k. Mao, *Physical Review*  
433 *B* **84** (10), 104110 (2011).
- 434 18. R. Bini and G. Pratesi, *Physical Review B* **55** (22), 14800-14809 (1997).
- 435 19. S. Umemoto, T. Yoshii, Y. Akahama and H. Kawamura, *Journal of Physics: Condensed*  
436 *Matter* **14** (44), 10675-10678 (2002).
- 437 20. L. Sun, W. Yi, L. Wang, J. Shu, S. Sinogeikin, Y. Meng, G. Shen, L. Bai, Y. Li, J. Liu,  
438 H. k. Mao and W. L. Mao, *Chemical Physics Letters* **473** (1-3), 72-74 (2009).
- 439 21. L. Sun, Z. Zhao, A. L. Ruoff, C.-S. Zha and G. Stupian, *Journal of Physics: Condensed*  
440 *Matter* **19** (42), 425206 (2007).
- 441 22. S. J. Clark, M. D. Segall, C. J. Pickard, P. J. Hasnip, M. I. J. Probert, K. Refson and M.  
442 C. Payne, *Zeitschrift für Kristallographie - Crystalline Materials* **220** (5-6), 567-570 (2005).
- 443 23. I. Kantor, V. Prakapenka, A. Kantor, P. Dera, A. Kurnosov, S. Sinogeikin, N.  
444 Dubrovinskaia and L. Dubrovinsky, *Review of Scientific Instruments* **83** (12), 125102 (2012).
- 445 24. See Supplemental Material for Methods, Supplemental Figures (S1-S5) and Tables (S1-  
446 S5), and References (28-33).
- 447 25. V. CrysAlisPro Software System, Rigaku Oxford Diffraction, Oxford, UK. Oxford, UK  
448 2014.
- 449 26. G. M. Sheldrick, *Acta Crystallographica Section A Foundations and Advances* **71** (1), 3-8  
450 (2015).
- 451 27. V. Petricek, M. Dusek and L. Palatinus, *Zeitschrift für Kristallographie* **229** (5), 345-352  
452 (2014).
- 453 28. N. Holtgrewe, E. Greenberg, C. Prescher, V. B. Prakapenka and A. F. Goncharov, *High*  
454 *Pressure Research* **39** (3), 457-470 (2019).
- 455 29. A. F. Goncharov, P. Beck, V. V. Struzhkin, R. J. Hemley and J. C. Crowhurst, *Journal of*  
456 *Physics and Chemistry of Solids* **69** (9), 2217-2222 (2008).
- 457 30. H. K. Mao, J. Xu and P. M. Bell, *Journal of Geophysical Research: Solid Earth* **91** (B5),  
458 4673-4676 (1986).

- 459 31. C. J. Pickard and R. J. Needs, *Journal of Physics: Condensed Matter* **23** (5), 053201  
460 (2011).
- 461 32. W. C. Hamilton, *Acta Crystallographica* **18** (3), 502-510 (1965).
- 462 33. A. Tkatchenko and M. Scheffler, *Physical Review Letters* **102** (7), 073005 (2009).
- 463 34. V. Labet, P. Gonzalez-Morelos, R. Hoffmann and N. W. Ashcroft, *The Journal of*  
464 *Chemical Physics* **136** (7), 074501 (2012).
- 465 35. I. Nakahata, N. Matsui, Y. Akahama and H. Kawamura, *Chemical Physics Letters* **302**  
466 (3), 359-362 (1999).

467

468